Nanoscale

PAPER

View Article Online
View Journal | View Issue

Check for updates

Cite this: *Nanoscale*, 2021, **13**, 10891

Tandem molecular self-assembly for selective lung cancer therapy with an increase in efficiency by two orders of magnitude†

Debin Zheng,[a] Jingfei Liu,[a] Yinghao Ding,[b] Limin Xie,[a] Yingying Zhang,[a] Yaoxia Chen,[a] Rong Peng,[a] Miao Cai,[a] Ling Wang,[b] Huaimin Wang, *[c] Jie Gao *[a] and Zhimou Yang *[a]

In situ self-assembly of prodrug molecules into nanomedicine can elevate the therapeutic efficacy of anticancer medications by enhancing the targeting and enrichment of anticancer drugs at tumor sites. However, the disassembly and biodegradation of nanomedicine after enrichment prevents the further improvement of the efficiency, and avoiding such disassembly and biodegradation remains a challenge. Herein, we rationally designed a tandem molecular self-assembling prodrug that could selectively improve the therapeutic efficacy of HCPT against lung cancer by two orders of magnitude. The tandem molecular self-assembly utilized an elevated level of alkaline phosphatase and reductase in lung cancer cells. The prodrug first self-assembled into nanofibers by alkaline phosphatase catalysis and was internalized more efficiently by lung cancer cells than free HCPT. The resulting nanofiber was next catalyzed by intracellular reductase to form a more hydrophobic nanofiber that prevented the disassembly and biodegradation, which further significantly improved the efficacy of HCPT against lung cancer both *in vitro* and *in vivo*.

Received 22nd February 2021,
Accepted 19th May 2021

DOI: 10.1039/d1nr01174j

rsc.li/nanoscale

Published on 24 mai 2021. Downloaded on 30/09/2024 05:31:22.

Introduction

Nanomedicine-based therapies have been studied extensively to address delivery problems with chemotherapeutics by improving the selectivity and increasing the drug concentration at desired locations.[1–5] For the time being, however, successfully translating nanomedicine in the clinic is still challenging.[6] One of the most significant factors delaying the clinical translation is the poor penetration of nanomedicines into tumors after intravenous injection.[7–9] In recent years, inspired by the approach of prodrugs that focus on enhancing the tumor permeability and penetrability of drugs,[10–13] *in situ* self-assembly (SA) of drug–peptide conjugates has been developed and emerged as a promising method in targeted drug delivery for cancer treatment by integrating the advantages of prodrugs and nanomedicines.[14–18] The drug–peptide conjugates serve as both prodrugs and nanomedicines by tumor site selective induction of SA, including environmental factors such as differences in pH,[19,20] temperature or ionic strength,[21–23] elevated levels of redox molecules such as GSH, H_2O_2 and other ROS species,[24,25] and overexpressed enzymes such as phosphatases,[26–29] proteases[30] and esterases.[31] These approaches work very well in enhancing the penetration of nanomedicines and enriching the concentration of drugs at desired sites.[10,32–34] However, the complex biological environment often causes the disassembly or biodegradation of the SA nanomedicine after enrichment in disease sites, which would lead to fast clearance of the drug and hinder the further improvement of the therapeutic efficacy. Avoiding such undesirable disassembly or biodegradation of the SA nanomedicine remains a challenge.[35–38]

Recently, *in situ* SA has evolved into tandem SA by connecting two steps of *in situ* SA. In several pioneering works, the first *in situ* SA triggered by enzymes overexpressed by disease sites promoted the targeting and cellular internalization of the SA nanomaterials, and the second tandem SA caused changes in the molecular chemical structure, morphology, or surface

[a]*State Key Laboratory of Medicinal Chemical Biology, Key Laboratory of Bioactive Materials, Ministry of Education, College of Life Sciences, Collaborative Innovation Center of Chemical Science and Engineering, and National Institute of Functional Materials, Nankai University, Tianjin 300071, P. R. China. E-mail: chemgaojie@nankai.edu.cn, yangzm@nankai.edu.cn*
[b]*College of Pharmacy, Nankai University, Tianjin 300071, P. R. China*
[c]*Key Laboratory of Precise Synthesis of Functional Molecules of Zhejiang Province, School of Science, Westlake University; Institute of Natural Sciences, Westlake Institute for Advanced Study, No. 18 Shilongshan Road, Hangzhou 310024, Zhejiang Province, P. R. China. E-mail: wanghuaimin@westlake.edu.cn*

†Electronic supplementary information (ESI) available: Synthesis of the compounds, NMR, HR-MS spectrum and CAC of the compounds, LC-MS spectrum and bio-TEM image; photographs of tumor tissue. See DOI: 10.1039/d1nr01174j

Published on 24 mai 2021. Downloaded on 30/09/2024 05:31:22.

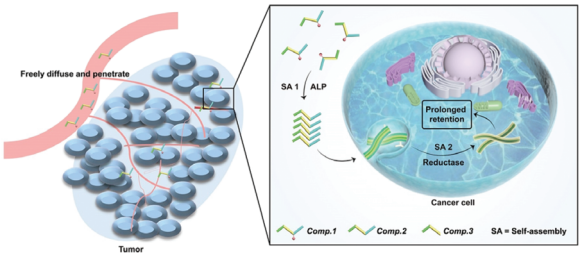

Scheme 1 Schematic of the tandem molecular self-assembly of the prodrug **Comp. 1**.

charge of the nanomaterial, which would ultimately lead to better selectivity or retention of the material.[39–41] Here, we described a novel tandem SA based approach to specifically deliver HCPT to lung tumors by *in situ* self-assembling HCPT at the tumor site and then preventing its disassembly and biodegradation inside the cancer cells by tandem SA (Scheme 1). The specific delivery and prolonged retention at lung tumor sites simultaneously improved the therapeutic efficacy of HCPT by two orders of magnitude.

Experimental

Peptide synthesis

The drug–peptide conjugates were prepared through SPPS. The F-moc group was removed by piperidine. HBTU served as the coupling reagents. The Fmoc-protected azobenzene group as amino acid can be used in SPPS. Finally, the liquid reagent composed of 95% of trifluoroacetic acid, 2.5% of $PhSCH_3$ and 2.5% of water was reacted with resin of crude products in the dark for 60 minutes. After purification and freeze-drying, pure products were obtained.

Tandem molecular self-assembly

The **Comp. 1** solution was firstly incubated at 37 °C for 5 min (pH = 7.4, 100 μM in PBS). The first step of self-assembly was induced by adding alkali phosphatase (ALP, 10 U mL^{-1}) into the work solution for 10 hours at 37 °C. After that, sodium dithionite (SDT, 20 mM) was added at 37 °C to initiate the second step of SA for 2 hours.

Bio-TEM

2×10^5 of lung cancer cells (A549) were seeded in a 6 well Petri dish. The cells were incubated with **Comp. 1** or **Comp. 2**, **4**, and **5** (100 μM) for 6 h. After that, the cells were collected using a cell scraper and then fixed with glutaraldehyde (2.5%), and finally observed by transmission electron microscopy (TEM).

Cell uptake

1×10^5 of A549 cells were seeded in a CLSM dish. After the cells adhered, the cells were treated with **Comp. 1**, **2**, **4** or **5** (100 μM) for 1, 2, 4 and 6 h, respectively. After that, the cells were incubated with Red dot 1 (1×, diluted with DMEM) to stain the nuclei for 5–10 min. The cells were washed with DMEM three times, and then CLSM was employed to detect fluorescence intensity. We utilized Image J to analyze relative fluorescence intensity.

Cell proliferation

Different cells were seeded in a 96-well plate and incubated with the compound for 48 hours after cell attachment. The medium containing the compound was removed. We used 100 μL of cold trichloroacetic acid solution (10%) to fix the cells at 4 °C overnight. We poured the fixative out and washed with water. We put it into an oven at 37 °C to dry it. Next, we used 0.4% SRB solution (100 μL) to stain the fixed cells for 25 min to form an SRB-bound protein, and then washed excessive SRB with 300 μL of AcOH solution (1%). After drying it, 10 mM Tris base solution was added into each well to solubilize the SRB-bound protein for 30 minutes. We measured the OD 570 nm *via* a microplate reader.

Tumor penetration study *in vivo*

All animal procedures were performed in accordance with the Guidelines for Care and Use of Laboratory Animals of Nankai University and approved by the Centre of Tianjin Animal Experiment Ethics Committee, and the accreditation number of the laboratory is SYXK(Jin) 2019-0003 promulgated by Tianjin Science and Technology Commission. BALB/c nude mice bearing about 200 mm^3 of A549 tumor were injected with **Comp. 6**, **7**, **8** and **9** (dose shown in Table S1,† *i.v.*). After 24 h, the mice were sacrificed to obtain the tumor tissue for frozen sections. The tumor samples were sectioned into 8 μm thickness on the equatorial plane. Then, the samples were fixed with acetone for 15 min and washed twice with PBS, 5% BSA blocking solution prevented nonspecific binding at room temperature for 1 h and the blood vessel was marked with the FITC-CD31 antibody for 1 h. After washing with PBS 3 times, the nucleus of the sample was stained with DAPI for 10 min.

Anti-tumor therapy

A549 tumor-bearing nude mice (tumor volume ~100 mm^3) were randomly divided into six groups (n = 5), then they were intravenously injected with **Comp. 1**, **2**, **4**, **5**, free HCPT and PBS at 1, 4, 7 and 10 days. Tumor volume and weight were monitored every 2 days for 19 days. After the whole observation period, the mice were sacrificed, and solid tumors were separated, and then fixed with 4% formaldehyde for hematoxylin and eosin (H&E) staining and immunofluorescence analysis.

Results and discussion

Prodrug design and synthesis

In our prior work,[41] we designed a peptide (GFFpYG–N═N–ERGD) that could self-assemble in a stepwise manner controlled by the catalysis of ALP and intracellular reductase. The ALP is reported to be highly overexpressed by a variety of

 This journal is © The Royal Society of Chemistry 2021

Published on 24 mai 2021. Downloaded on 30/09/2024 05:31:22.

cancer cells and mainly located on or outside the surface of the cell membrane. Meanwhile, lung cancer cells exhibit elevated expression of intracellular reductase. The peptide therefore could tandemly respond to those enzymes and selectively formed nanomaterials inside lung cancer cells. In this study, we conjugated 10-hydroxycamptothecin (HCPT) with the above-mentioned peptide. The obtained molecule HCPT–GFFpYG–N═N–ERGD (**Comp. 1** in Fig. 1A) was a prodrug with tandem self-assembling ability.

We first synthesized the Fmoc-azo-benzene (**Comp. S2**) as the reductase responsive group and glutaric anhydride modified 10-hydroxycamptothecin as the drug capping group. Both of them can be directly used in solid phase peptide synthesis (SPPS). Therefore, after standard SPPS and purification by reversed-phase high-performance liquid chromatography (HPLC), we obtained the pure compound of **Comp. 1**. Other control compounds were synthesized *via* a comparable process, including HCPT–GFFYG–N═N–ERGD (only reductase-response, namely **Comp. 2**), HCPT–GFFpYGERGD (only ALP-response, namely **Comp. 4**), and HCPT–GFFYGERGD (non-ALP- and non-reductase-response, namely **Comp. 5**).

Enzyme instructed tandem self-assembly

A yellow clear solution (100 μM, 0.018 wt%) was formed by **Comp. 1** in phosphate buffered saline (PBS, pH = 7.4), which was lower than its critical aggregation concentration (CAC = 198.01 μM, Fig. S11A†). The transmission electron microscopy (TEM) images showed non-assembled structures in the PBS solution of **Comp. 1** (Fig. S12A†). It remained a yellow clear solution (Fig. 1B), after adding ALP (10 U mL^{-1}) to the solution of **Comp. 1** for 10 hours at 37 °C. The LC-MS trace indicated that **Comp. 1** could be converted into **Comp. 2** by ALP (Fig. S13†). The value of CAC decreased to 53.3 μM (Fig. S10B†), due to changes in hydrophobicity. We observed nanofibers with diameters of 8–14 nm in the resulting solution of **Comp. 2** through TEM (Fig. 1B). After the addition of sodium dithionite ($Na_2S_2O_4$, 20 mM), which was used to mimic reductase,[42] the yellow solution of **Comp. 2** became light yellow and more transparent within 2 hours, probably due to the conversion of azo benzene to aniline (Fig. 1C). The LC-MS trace shown in Fig. S14† revealed that most of the **Comp. 2** had been converted into **Comp. 3**. The TEM images in Fig. 1C showed nanofibers with diameters of 6–10 nm. These observations demonstrated the tandem molecular self-assembling behavior of **Comp. 1** catalyzed by ALP and reductase.

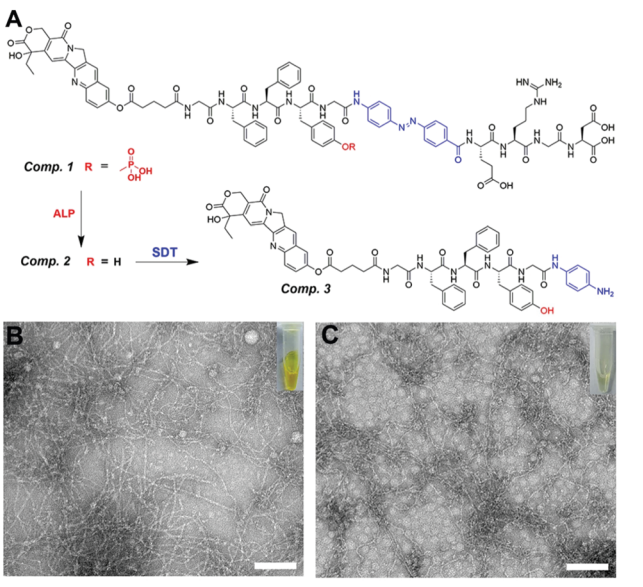

Fig. 1 (A) Enzyme instructed chemical structure conversions from **Comp. 1** to **2** by ALP and then **Comp. 2** to **3** by SDT. TEM and optical images of (B) **Comp. 2** acquired by ALP catalysis and (C) **Comp. 3** acquired by SDT catalysis, scale bar = 100 μm.

Intracellular tandem self-assembly in lung cancer cells

To study whether tandem molecular SA could enrich HCPT in lung cancer cells, we utilized confocal laser scanning microscopy (CLSM) and bio-TEM to reveal the distribution of different compounds in live A549 cells. As shown in Fig. 2A, we could observe obvious green fluorescence dots in the cytoplasm of A549 cells after incubating the cells with **Comp. 1** (100 μM) for 6 hours, while the cells treated with the same amount of control compounds (**Comp. 2**, **4** or **5**) or free HCPT showed much weaker fluorescence. The quantified fluorescence intensity from CLSM images could indicate the relative cellular concentration of different compounds. As shown

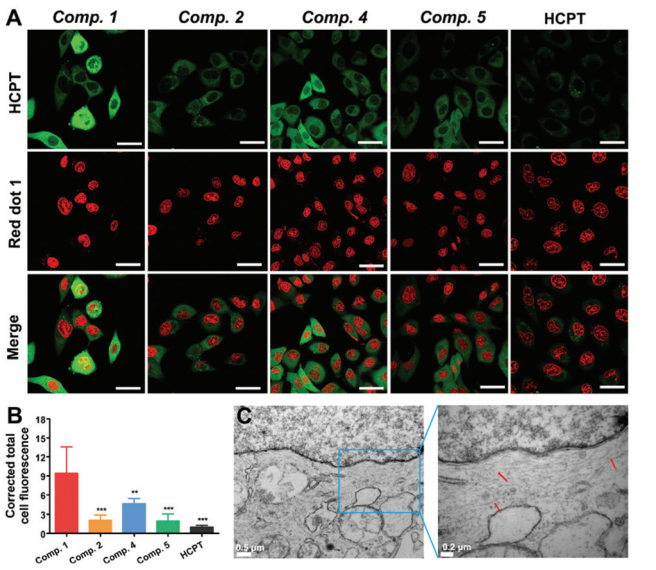

Fig. 2 (A) CLSM images of A549 cells treated with 100 μM of **Comp. 1**, **2**, **4**, **5** and HCPT for 6 h ($\lambda_{exc.}$ = 405 nm for green channel, and $\lambda_{exc.}$ = 633 nm for red channel, white scale bar = 25 μm). (B) Corrected total cell fluorescence (CTCF, quantified from the gray scale of (A), one-way ANOVA, compared to the **Comp. 1** group, mean ± SD, ***P < 0.001, **P < 0.01, N = 5). (C). Bio-TEM image of A549 cells after administration of **Comp. 1** for 6 hours, the red arrow points to nanofibers.

Published on 24 mai 2021. Downloaded on 30/09/2024 05:31:22.

in Fig. 2B, the **Comp. 1** group exhibited the highest fluorescence intensity, which indicated the highest cellular drug concentration. Meanwhile, the free HCPT group showed the least fluorescence intensity, mainly due to the extremely water-insoluble and poor cellular internalization efficiency of the molecule. Interestingly, the **Comp. 4** group showed higher fluorescence intensity than the groups of **Comp. 2** and **5**. According to many studies, the ALP catalyzed self-assembling molecules were internalized much more than the unassembled ones by the ALP over-expressing cancer cells,[43] because they entered the cells through endocytosis. Since both **Comp. 1** and **4** are ALP responsive self-assembling molecules, it is reasonable that these two molecules are internalized by the A549 cells more than non-ALP responsive molecules. However, the fluorescence intensity of **Comp. 4** was still much lower than that of **Comp. 1**. The reason for the differences in fluorescence intensity could be attributed to two factors: more cellular internalization and less biodegradation inside the cells.

In order to elucidate the reason, we monitored the fluorescence intensity of cells treated with different compounds in a time dependent manner. As shown in Fig. S16 and S17,† after treating the cells with different compounds for a short time period (2 hours), the fluorescence intensities of the **Comp. 1** and **4** group were already larger than those of other groups, indicating that the cells could uptake **Comp. 1** and **4** more than other compounds. However, since the CAC value for **Comp. 4** after adding ALP was larger than that for **Comp. 1** (102.6 μM, Fig. S11C and D†), which indicated that its self-assembling ability was weaker than that of **Comp. 1**, the cellular uptake of **Comp. 4** was less than that of **Comp. 1**. After a relatively long time of treatment (4 hours), the differences were further increased between the **Comp. 1** group and other groups. We then removed the compounds from the cell culture medium to evaluate the biodegradation of the compounds inside the cell. As shown in Fig. S18,† after removing the compounds for 4 hours, the fluorescence intensity of **Comp 2**, **4** and **5** decreased a lot, while **Comp. 1** and HCPT remained unchanged, suggesting that **Comp. 1** and HCPT could resist the biodegradation inside the cells. The chemical structure of the self-assembled molecules changes under the catalysis of reductase inside the cell. The shedding of hydrophilic ERGD will cause the formation of more hydrophobic nanofibers, which may be one of the reasons for the resistance to biodegradation. Furthermore, as shown in Fig. 2C, the bio-TEM images of A549 cells post administration of **Comp. 1** for 6 hours exhibited short nanofibers with diameters of 7–10 nm in the cytoplasm. In contrast, no such nanostructures were found in the other control groups (Fig. S15†). These observations demonstrated the formation of the second nanofiber of **Comp. 1** and its strong anti-biodegradation ability after the tandem SA process, indicating that tandem SA could significantly enrich HCPT in A549 cells for a longer time because of more internalization and stronger biodegradation resistance of **Comp. 1**.

We then studied the selectivity of the tandem self-assembled nanomedicines. We chose three cancer cell lines with overexpression of ALP on the cell membrane and lower expression of reductase inside the cell than the A549 cell (HeLa, MCF-7 and PC-3) and treated them with **Comp. 1** for 6 hours. The confocal images in Fig. S19† show that weak green fluorescence was observed in the cytoplasm of HeLa, MCF-7 and PC-3 cells. The quantified fluorescence intensities (Fig. S20†) of these cell lines were significantly lower than those of A549 cells. These observations indicated that **Comp. 1** had excellent selectivity to A549 cells because of the over-expression of both ALP and reductase in lung cancer cells.

The above explorations showed that the tandem self-assembling strategy could effectively retain SA nanomedicines for a longer time inside the cancer cells, which might improve the efficiency of drugs to inhibit cancer cells. We therefore examined the cytotoxicity of **Comp. 1** and other compounds against A549 cells. Compared to **Comp. 2**, **4**, **5** and free HCPT with IC_{50} values of 4.9 μM, 3.5 μM, 4.7 μM, and 5.7 μM, respectively, **Comp. 1** exhibited the most remarkable suppression to A549 cells with an IC_{50} value as low as 63 nM (Fig. 3A). The inhibition efficacy of A549 cells treated with **Comp. 1** was about 91 fold higher than that of free HCPT and 45–75 fold higher than that of other compounds, demonstrating the strong potency of **Comp. 1** for killing A549 cells. Next, we examined the ratio of the IC_{50} value for **Comp. 1** and free HCPT. As shown in Fig. 3B, the IC_{50} values of **Comp. 1** against PC-3, MCF-7 and HeLa cells were only 2.4, 0.8 and 22 fold higher than that of free HCPT, respectively. Furthermore, we tested the compatibility and cell uptake of **Comp. 1** towards the LO2 normal cells, as shown in Fig. S21.† The toxicity and cell uptake of **Comp. 1** was not higher than that of free HCPT towards LO2 cells at the same concentration. These results clearly showed the excellent selectivity of **Comp. 1** to lung cancer cells and demonstrated that the improved potency of **Comp. 1** was due to the tandem self-assembling process triggered by the elevated level of ALP and reductase in lung cancer cells.

Evaluation of penetration, accumulation and retention of tandem molecules at tumor sites

According to many studies, the efficacy of nanomedicines depends on their ability of penetration, accumulation and retention at the tumor site.[10] Tandem *in situ* self-assembly of prodrugs enables the drug to penetrate and further retain.

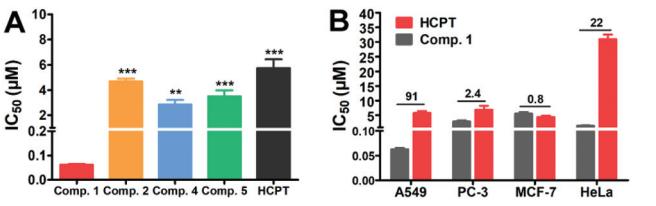

Fig. 3 Cytotoxicity of the tandem self-assembling prodrug. (A) IC_{50} value of A549 cells treated with **Comp. 1**, **2**, **4**, **5** and free HCPT. (B) IC_{50} value of **Comp. 1** and HCPT to different cell lines. (One-way ANOVA, compared to the **Comp. 1** group, mean ± SD, $^{***}P < 0.001$, $^{**}P < 0.01$. $N = 3$.)

This journal is © The Royal Society of Chemistry 2021

Published on 24 mai 2021. Downloaded on 30/09/2024 05:31:22.

Inspired by this, we evaluated the penetration and retention of **Comp. 1** on multicellular spheroids (MCSs) of A549 cells that mimic solid tumors. The MCSs were incubated with different compounds (100 μM) for 6 hours. As shown in Fig. S22,† green fluorescence signals of **Comp. 1** were observed at different depths and reached the interior of MCSs (80 μm). Since **Comp. 1** was a small hydrophilic molecule, it could diffuse freely inside the MCSs and then tandemly self-assemble to form stable nanofibers instructed by ALP and reductase, which further improved the accumulation and retention in the MCSs. As a comparison, the fluorescence intensities of the A549 MCSs incubated with **Comp. 2**, **4** and **5** were much lower than that in the **Comp. 1** group at the corresponding depths.

We then investigated the body distribution of the tandem self-assembling molecules on A549 tumor-bearing BALB/c nude mice (Table S1†). The cyanine-5.5 (Cy-5.5) labeled tandem self-assembling molecule (**Comp. 6**, Fig. S6†) and three control compounds without tandem SA were synthesized and utilized for IVIS Lumina II imaging (**Comp. 7**, **8** and **9**, Fig. S8–S10†). As shown in Fig. 4A, **Comp. 6**, **8** and **9** achieved fast whole-body distribution within 4 hours with high concentration due to excellent hydrophilicity. 24 hours after the injection, we observed the strongest fluorescence intensity from **Comp. 6** at the tumor site and the fluorescence signals could last up to 36 hours. The fluorescence intensities of **Comp. 8** and **9** were weaker than that of **Comp. 6** after at 8 hours and later disappeared within 36 hours. Meanwhile, only weak fluorescence could be observed in the **Comp. 7** group due to the poor solubility of the molecule. These results demonstrated the excellent tumor accumulation and retention characteristic of the tandem self-assembling molecule **Comp. 6**. Furthermore, the excised normal organs and tumor tissues were harvested 36 hours post injection, in order to assess the distribution of different compounds *ex vivo*. As shown in Fig. S23,† **Comp. 6** possessed the highest retention and accumulation capacity among all groups, which is consistent with the results of IVIS images *in vivo*. We also observed that **Comp. 6**, **8** and **9** were mainly metabolized by the kidneys, while the poorly soluble **Comp. 7** was also metabolized by the liver in addition to the kidneys. We also obtained frozen sections of the excised solid tumors after intravenously injecting **Comp. 6–9** for 24 hours. As shown in Fig. 4B and Fig. S24,† **Comp. 6** (red fluorescence) could efficiently retain in larger tumor areas compared to other control compounds without tandem SA. As a result, it was concluded that the tandem molecular SA strategy can improve the ability of accumulation, retention and penetration of the prodrug.

Evaluation of anti-tumor efficacy and biosafety *in vivo*

Encouraged by the efficient cancer cell inhibition and excellent tumor penetration, accumulation and retention capacity, we evaluated the therapeutic potential of the tandem self-assembling prodrug to the solid tumor in a BALB/c nude mouse model bearing A549 cells. Six groups of mice with an average tumor size of 100 mm^3 were treated with **Comp. 1**, **2**, **4**, **5**, free HCPT and PBS *via* the tail vein (once every three days, 3 mg kg^{-1} HCPT-equivalent dose, Table S2,† $N = 5$). As shown in Fig. 5B and S25,† the tumor volume began to decrease after the first administration of **Comp. 1**. Tumor volume slightly increased to 189 mm^3 at the 19th day. The tumor volume in the groups of **Comp. 2**, **4**, **5** and free HCPT were about 423 mm^3, 451 mm^3, 451 mm^3 and 499 mm^3, respectively, which were more than 2.5 fold larger than that of the **Comp. 1** group. The tumor volume of PBS groups reached about 951 mm^3 at the 19th day, which was 5-fold larger compared to

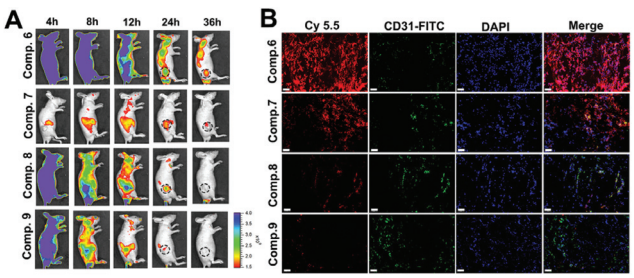

Fig. 4 (A) Representative pictures of NIR-fluorescence imaging of A549 tumor bearing nude mice with the treatment of **Comp. 6**, **7**, **8** and **9** at different time points after the intravenous administration. (B) CLSM images of cryo-sections of A549 tumor tissue after intravenous administration of **Comp. 6**, **7**, **8** and **9** for 24 h, the DAPI-stained nucleus (blue channel), FITC-CD31-stained blood vessel (green channel), Cy5.5 (red channel), and overlay image, scale bar = 50 μm.

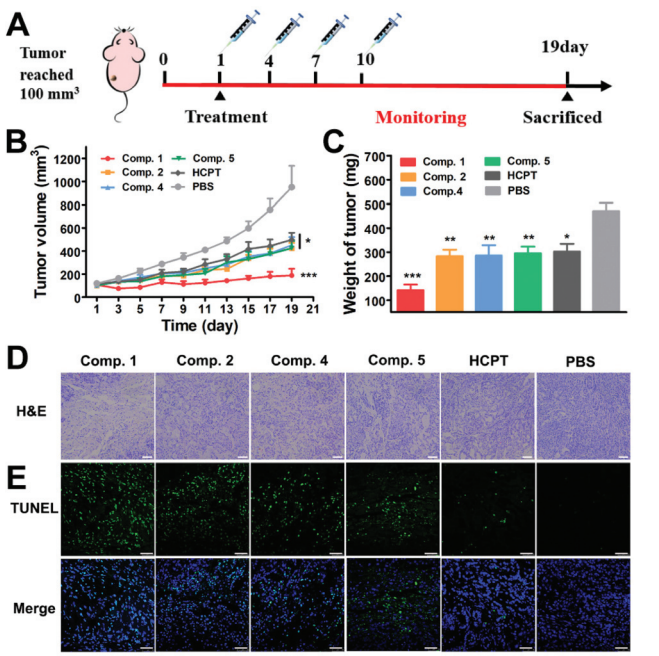

Fig. 5 (A) Treatment schedule for inhibition of A549 tumors in BALB/c nude mice. The treatment of A549 tumor bearing nude mice by the intravenous injection of **Comp. 1**, **2**, **4**, **5**, HCPT and PBS at a dose equaled 3 mg kg^{-1} equivalent of HCPT. (B) Tumor volume. (C) Tumor weight. (D) H&E staining of tumor tissues, scale bar = 100 μM. (E) TUNEL analyses of tumor tissues, scale bar = 50 μM.

Published on 24 mai 2021. Downloaded on 30/09/2024 05:31:22.

the **Comp. 1** group. Meanwhile, as shown in Fig. 5C and Fig. S26B,† the average tumor weight of the **Comp. 1** group was 141.5 mg, which was significantly lower than that of the other groups. We then verified whether **Comp.1** could improve the survival rate relative to free HCPT. The BLAB/c nude mice bearing A549 tumors were randomly divided into three groups (N = 6), including **Comp. 1**, free HCPT and PBS groups. After the administration of therapeutic agents and monitoring for 34 days (Fig. S27†), the first death in the PBS group occurred on the 23rd day, and all the mice died on the 27th day. Meanwhile, the first death in the free HCPT group occurred on the 27th day, and all of the mice in this group died on the 31st day. However, only one mouse in the **Comp. 1** group died on the 29th day during the entire monitoring period. These results clearly demonstrated that the tandem self-assembling prodrug inhibited the growth of lung tumor efficiently and improved the survival rate of animals greatly.

We further used Hematoxylin and Eosin (H&E) staining and terminal deoxynucleotidyl transferase-mediated dUTP-biotin nick end-labeling assay (TUNEL) to assess the anti-tumor efficacy of different compounds. All groups of mice were sacrificed on the 19th day after administration, and tumor tissues were harvested. H&E staining of tumor tissue (Fig. 5D) in the PBS group presented intact tumor tissue morphology, where compact tumor cells speckled with large amounts of extracellular matrix maintaining cancer cell normal growth. Among the groups treated with different prodrugs and free HCPT, the **Comp. 1** group displayed the largest tissue necrotic area and the least tumor cellularity, exhibiting the most prominent anti-tumor efficacy of tandem self-assembling prodrugs. Meanwhile, as shown in Fig. 5E, the results of TUNEL also showed that **Comp. 1** induced a large number of tumor cell apoptosis, while other compounds or the free HCPT could not. These results together demonstrated that tandem molecular SA could significantly improve the tumor inhibition efficiency of anticancer drugs.

In order to test the biosafety of various therapeutic agents used in this study, body weights of mice were continuously recorded for 19 days (once every two days). As shown in Fig. S26A,† all groups showed no obvious body weight change during the whole treatment period. In addition, the main organs (heart, liver, spleen, lungs, and kidneys) of the mice were collected after completing the treatment monitoring. H&E staining images (Fig. S28†) show that there were no obvious cell damage and histopathological changes compared to the saline group. To further assess the biosafety of various formulations of HCPT *in vivo*, normal BALB/c nude mice were injected in all therapeutic agents three times (3 mg kg^{-1} HCPT-equivalent dose, once every two days), and the blood samples were collected and analyzed to obtain the clinical blood parameters and blood biochemical values. As shown in Fig. S29,† the clinical hematology markers of **Comp. 1**, **2**, **4**, **5** and free HCPT groups, including red blood cell (RBC) count, white blood cell (WBC) count, hemoglobin (HGB), and platelets (PLT) count showed a negligible difference compared to the PBS group, and the sample detection values are all within the index reference range. For the blood biochemical index, the levels of aspartate transaminase (AST), alanine transaminase (ALT), alkaline phosphatase (ALP), total bilirubin (TBIL) and direct bilirubin (DBIL) represented the liver parenchymal injury. The levels of urea (UA), blood urea nitrogen (BUN), and creatinine (CRE) were commonly used to evaluate the kidney condition. As shown in Fig. S30,† although there is a certain difference in the detection values for each group, all the values of the above blood biochemistry indicators are within the normal reference range of the index. These observations demonstrated trustworthy biosafety of the peptide-based prodrug with tandem molecular SA.

Conclusions

In summary, we developed a tandem molecular SA strategy to significantly improve the anti-tumor efficiency of HCPT by two orders of magnitude. The designed peptide–HCPT prodrug could self-assemble into fibrous nanomedicine by ALP catalysis and thus be up-taken by lung cancer cells much more than free HCPT. Then, the internalized nanofibers could transform into another nanomedicine by reductase instructed self-assembling, which prevented the degradation or disassembly of the nanomedicine. At the cellular level, the tandem self-assembled prodrug had good selectivity and greatly increased the IC_{50} of HCPT due to the increased internalization and retention of the drug. As a result, it could improve the tumor accumulation and retention of the drug *in vivo*, which effectively inhibited the lung tumor growth without side effects. We envision that the tandem molecular SA strategy can facilitate the development of selective and effective nanomedicines for precise chemotherapeutics.

Author contributions

D. B. Zheng, J. F. Liu, Y. H. Ding, Y. Y. Zhang and R. Peng synthesized and characterized the compounds. D. B. Zheng, J. F. Liu and L. M. Xie performed the cell imaging and experiments. D. B. Zheng, Y. X. Chen and M. Cai analysed the results and performed the scheme illustration. L. Wang, H. M. Wang, J. Gao and Z. M. Yang guided the research and wrote the manuscripts.

Conflicts of interest

There are no conflicts to declare.

Acknowledgements

This work was supported by the National Science Fund for Distinguished Young Scholars (31825012), the NSFC (51773097, 82022038, and 31961143004), and the Young Elite Scientists Sponsorship Program by Tianjin (TJSQNTJ-2017-16).

 This journal is © The Royal Society of Chemistry 2021

Published on 24 mai 2021. Downloaded on 30/09/2024 05:31:22.

Notes and references

1 J. J. Shi, P. W. Kantoff, R. Wooster and O. C. Farokhzad, *Nat. Rev. Cancer*, 2017, **17**, 20–37.
2 E. Blanco, H. Shen and M. Ferrari, *Nat. Biotechnol.*, 2015, **33**, 941–951.
3 E. K. Lim, T. Kim, S. Paik, S. Haam, Y. M. Huh and K. Lee, *Chem. Rev.*, 2015, **115**, 327–394.
4 K. Sato, M. P. Hendricks, L. C. Palmer and S. I. Stupp, *Chem. Soc. Rev.*, 2018, **47**, 7539–7551.
5 J. Xie, S. Lee and X. Chen, *Adv. Drug Delivery Rev.*, 2010, **62**, 1064–1079.
6 V. J. Venditto and F. C. Szoka, *Adv. Drug Delivery Rev.*, 2013, **65**, 80–88.
7 M. F. Flessner, J. Choi, K. Credit, R. Deverkadra and K. Henderson, *Clin. Cancer Res.*, 2005, **11**, 3117–3125.
8 C. H. Heldin, K. Rubin, K. Pietras and A. Ostman, *Nat. Rev. Cancer*, 2004, **4**, 806–813.
9 Y. Matsumoto, J. W. Nichols, K. Toh, T. Nomoto, H. Cabral, Y. Miura, R. J. Christie, N. Yamada, T. Ogura, M. R. Kano, Y. Matsumura, N. Nishiyama, T. Yamasoba, Y. H. Bae and K. Kataoka, *Nat. Nanotechnol.*, 2016, **11**, 533–538.
10 Q. Zhou, S. Shao, J. Wang, C. Xu, J. Xiang, Y. Piao, Z. Zhou, Q. Yu, J. Tang, X. Liu, Z. Gan, R. Mo, Z. Gu and Y. Shen, *Nat. Nanotechnol.*, 2019, **14**, 799–809.
11 R. W. Chakroun, F. Wang, R. Lin, Y. Wang, H. Su, D. Pompa and H. Cui, *ACS Nano*, 2019, **13**, 7780–7790.
12 F. H. Wang, H. Su, R. Lin, R. W. Chakroun, M. K. Monroe, Z. Y. Wang, M. Porter and H. G. Cui, *ACS Nano*, 2020, **14**, 10083–10094.
13 S. Li, Y. Zhang, S. H. Ho, B. Li, M. Wang, X. Deng, N. Yang, G. Liu, Z. Lu, J. Xu, Q. Shi, J. Y. Han, L. Zhang, Y. Wu, Y. Zhao and G. Nie, *Nat. Biomed. Eng.*, 2020, **4**, 732–742.
14 H. Wang, Z. Feng and B. Xu, *Adv. Drug Delivery Rev.*, 2017, **110–111**, 102–111.
15 C. Liang, X. Yan, R. Zhang, T. Xu, D. Zheng, Z. Tan, Y. Chen, Z. Gao, L. Wang, X. Li and Z. Yang, *J. Controlled Release*, 2020, **317**, 109–117.
16 P. Schiapparelli, P. Zhang, M. Lara-Velazquez, H. Guerrero-Cazares, R. Lin, H. Su, R. W. Chakroun, M. Tusa, A. Quinones-Hinojosa and H. Cui, *J. Controlled Release*, 2020, **319**, 311–321.
17 T. Wang, Y. Li, J. Wang, Y. Xu, Y. Chen, Z. Lu, W. Wang, B. Xue, Y. Li and Y. Cao, *ACS Biomater. Sci. Eng.*, 2020, **6**, 6800–6807.
18 Q. Guo, Y. Liu, G. Mu, L. Yang, W. Wang, J. Liu and J. Liu, *Biomater. Sci.*, 2020, **8**, 5638–5646.
19 Y. Cong, L. Ji, Y. J. Gao, F. H. Liu, D. B. Cheng, Z. Y. Hu, Z. Y. Qiao and H. Wang, *Angew. Chem., Int. Ed.*, 2019, **58**, 4632–4637.
20 R. Kubota, S. Torigoe, S. Liu and I. Hamachi, *Chem. Lett.*, 2020, **49**, 1319–1323.
21 P. Nasrollahi, K. Khajeh, E. Tamjid, M. Taleb, M. Soleimani and G. J. Nie, *Artif. Cells, Nanomed., Biotechnol.*, 2018, **46**, 1170–1177.
22 W. Ji, C. Yuan, S. Zilberzwige-Tal, R. Xing, P. Chakraborty, K. Tao, S. Gilead, X. Yan and E. Gazit, *ACS Nano*, 2019, **13**, 7300–7309.
23 Y. Li, Q. Zou, C. Yuan, S. Li, R. Xing and X. Yan, *Angew. Chem., Int. Ed.*, 2018, **57**, 17084–17088.
24 Q. Wu, Z. G. He, X. Wang, Q. Zhang, Q. C. Wei, S. Q. Ma, C. Ma, J. Li and Q. G. Wang, *Nat. Commun.*, 2019, **10**, 240.
25 X. Xia, X. Yang, P. Huang and D. Yan, *ACS Appl. Mater. Interfaces*, 2020, **12**, 18301–18308.
26 H. M. Wang, Z. Q. Q. Feng and B. Xu, *Angew. Chem., Int. Ed.*, 2019, **58**, 5567–5571.
27 J. F. Shi, G. Fichman and J. P. Schneider, *Angew. Chem., Int. Ed.*, 2018, **57**, 11188–11192.
28 Q. Yao, F. Lin, X. Fan, Y. Wang, Y. Liu, Z. Liu, X. Jiang, P. R. Chen and Y. Gao, *Nat. Commun.*, 2018, **9**, 5032.
29 J. Zhang, S. Liu, H. Li, X. Tian and X. Li, *Langmuir*, 2020, **36**, 11316–11323.
30 H. W. An, L. L. Li, Y. Wang, Z. Wang, D. Hou, Y. X. Lin, S. L. Qiao, M. D. Wang, C. Yang, Y. Cong, Y. Ma, X. X. Zhao, Q. Cai, W. T. Chen, C. Q. Lu, W. Xu, H. Wang and Y. Zhao, *Nat. Commun.*, 2019, **10**, 4861.
31 X. Han, K. Cheng, Y. Xu, Y. Wang, H. Min, Y. Zhang, X. Zhao, R. Zhao, G. J. Anderson, L. Ren, G. Nie and Y. Li, *J. Am. Chem. Soc.*, 2020, **142**, 2490–2496.
32 Y. B. Cai, H. S. Shen, J. Zhan, M. L. Lin, L. H. Dai, C. H. Ren, Y. Shi, J. F. Liu, J. Gao and Z. M. Yang, *J. Am. Chem. Soc.*, 2017, **139**, 2876–2879.
33 D. B. Cheng, D. Wang, Y. J. Gao, L. Wang, Z. Y. Qiao and H. Wang, *J. Am. Chem. Soc.*, 2019, **141**, 4406–4411.
34 Z. Feng, X. Han, H. Wang, T. Tang and B. Xu, *Chem*, 2019, **5**, 2442–2449.
35 T. Suma, J. Cui, M. Mullner, S. Fu, J. Tran, K. F. Noi, Y. Ju and F. Caruso, *J. Am. Chem. Soc.*, 2017, **139**, 4009–4018.
36 G. Rong, C. Wang, L. Chen, Y. Yan and Y. Cheng, *Sci. Adv.*, 2020, **6**, eaaz1774.
37 B. C. Evans, K. M. Hocking, K. V. Kilchrist, E. S. Wise, C. M. Brophy and C. L. Duvall, *ACS Nano*, 2015, **9**, 5893–5907.
38 C. Palm, M. Jayamanne, M. Kjellander and M. Hallbrink, *Biochim. Biophys. Acta*, 2007, **1768**, 1769–1776.
39 J. Zhan, Y. Cai, S. He, L. Wang and Z. Yang, *Angew. Chem., Int. Ed.*, 2018, **57**, 1813–1816.
40 W. Tang, Z. Zhao, Y. Chong, C. Wu, Q. Liu, J. Yang, R. Zhou, Z. X. Lian and G. Liang, *ACS Nano*, 2018, **12**, 9966–9973.
41 D. Zheng, Y. Chen, S. Ai, R. Zhang, Z. Gao, C. Liang, L. Cao, Y. Chen, Z. Hong, Y. Shi, L. Wang, X. Li and Z. Yang, *Research*, 2019, **2019**, 4803624.
42 F. Zhou, T. Fu, Q. Huang, H. Kuai, L. Mo, H. Liu, Q. Wang, Y. Peng, D. Han, Z. Zhao, X. Fang and W. Tan, *J. Am. Chem. Soc.*, 2019, **141**, 18421–18427.
43 J. Gao, J. Zhan and Z. Yang, *Adv. Mater.*, 2020, **32**, e1805798.